Atmospheric
Chemistry
and Physics

Open Access

The role of aerosol in altering North Atlantic atmospheric circulation in winter and its impact on air quality

F. S. R. Pausata[1,2,*], **M. Gaetani**[1,**], **G. Messori**[2], **S. Kloster**[3], **and F. J. Dentener**[1]

[1]European Commission, Joint Research Centre, Institute for Environment and Sustainability, Ispra (VA), Italy
[2]Department of Meteorology, Stockholm University and Bolin Centre for Climate Research, Stockholm, Sweden
[3]Land in the Earth System, Max Planck Institute for Meteorology, Hamburg, Germany
[*]now at: Department of Meteorology, Stockholm University and Bolin Centre for Climate Research, Stockholm, Sweden
[**]now at: LATMOS-IPSL, Université Pierre et Marie Curie, Paris, France

Correspondence to: F. S. R. Pausata (francesco.pausata@misu.su.se)

Abstract. Numerical model scenarios of future climate depict a global increase in temperatures and changing precipitation patterns, primarily driven by increasing greenhouse gas (GHG) concentrations. Aerosol particles also play an important role by altering the Earth's radiation budget and consequently surface temperature. Here, we use the general circulation aerosol model ECHAM5-HAM, coupled to a mixed layer ocean model, to investigate the impacts of future air pollution mitigation strategies in Europe on winter atmospheric circulation over the North Atlantic. We analyse the extreme case of a maximum feasible end-of-pipe reduction of aerosols in the near future (2030), in combination with increasing GHG concentrations. Our results show a more positive North Atlantic Oscillation (NAO) mean state by 2030, together with a significant eastward shift of the southern centre of action of sea-level pressure (SLP). Moreover, we show a significantly increased blocking frequency over the western Mediterranean.

By separating the impacts of aerosols and GHGs, our study suggests that future aerosol abatement may be the primary driver of both the eastward shift in the southern SLP centre of action and the increased blocking frequency over the western Mediterranean. These concomitant modifications of the atmospheric circulation over the Euro-Atlantic sector lead to more stagnant weather conditions that favour air pollutant accumulation, especially in the western Mediterranean sector. Changes in atmospheric circulation should therefore be included in future air pollution mitigation assessments. The indicator-based evaluation of atmospheric circulation changes presented in this work will allow an objective first-order assessment of the role of changes in wintertime circulation on future air quality in other climate model simulations.

1 Introduction

Future climate scenarios indicate a global increase in temperatures and changes in the hydrological cycle, mainly driven by increasing greenhouse gas (GHG) concentrations (IPCC, 2013). However, GHGs are not the only climate factor responsible for changing the Earth's radiation budget. Aerosol particles ("aerosols") also play a very important role in altering climate, both directly – by scattering and absorbing solar radiation – and indirectly – by influencing cloud radiative properties (cloud albedo effect; Twomey, 1977), and cloud formation and duration (cloud lifetime effect; Albrecht, 1989). The direct effect of non-absorbing aerosols – such as sulphates – produces an overall cooling of the atmosphere, while partly absorbing aerosols – such as black and organic carbon – can lead to either a cooling or a warming, depending on the aerosols' properties and underlying albedo.

Global climate models can realistically reproduce the temperature trend of the last century only when the radiative impacts of both GHGs and aerosols are included (Gleckler et al., 2008; Nazarenko and Menon, 2005; Roeckner et al., 1999; IPCC 2013). Therefore, increasing GHG concentrations as well as changes in aerosol abundance will control future climate and the associated atmospheric circulation

variations. High aerosol concentrations can also have severe impacts on human health (Lim et al., 2012; WHO, 2013). Consequently, air-quality standards have been introduced in many polluted regions to regulate harmful aerosol concentrations, and the upward trends in aerosol emissions in the most polluted regions are expected to stabilize or reverse. Hence, a realistic assessment of on-going and future climate change relies on our ability to predict trends in both GHG and aerosol emissions, the resulting concentrations and their combined effect on climate.

Most of the GHGs are long-lived and have a geographically homogeneous climate forcing. On the other hand, aerosol concentrations are highly inhomogeneous, since they are locally controlled by a combination of primary or precursor emissions, chemical reactions as well as large-scale atmospheric circulation, and their impacts can have short-term repercussions on climate (Shindell et al., 2012). Furthermore, atmospheric circulation changes themselves can feedback on air quality. Modelling and observational analyses suggest that a warming climate degrades air quality, with increasing surface O_3 and particulate matter abundance in many populated regions (Fiore et al., 2012). Kloster et al. (2009), for example, used a coupled chemistry–atmosphere general circulation model to show that climate change alone would worsen the air pollution by aerosols in many world regions.

Several other studies have demonstrated that local-to-regional scale pollutant concentrations can be influenced by large-scale atmospheric circulation patterns (Eckhardt et al., 2003; Christoudias et al., 2012; Barnes and Fiore, 2013; Pausata et al., 2012, 2013), such as the North Atlantic Oscillation (NAO). Pausata et al. (2013) have shown how positive shifts in the NAO in winter over the North Atlantic penalize cities lying in the Mediterranean area, making it necessary for these countries to enforce more stringent emission reduction measures. This is of particular importance in view of a potential shift towards positive NAO regimes under future climate conditions.

The NAO commonly refers to swings in the atmospheric pressure difference between the subpolar and subtropical North Atlantic, and is the leading mode of winter atmospheric variability in the North Atlantic. The standard NAO index (NAOI) is defined as the difference in normalized mean sea-level pressure (SLP) between the Azores (or Portugal) and Iceland (Walker and Bliss, 1932), and determines climate variability from the eastern seaboard of North America to Siberia and from the Arctic to the subtropical Atlantic. The NAO featured an upward trend of over 1 standard deviation in the 1980s and 1990s compared to the 1951–1970 winter mean (data available in http://www.cgd.ucar.edu/staff/jhurrell/naointro.html). Recent multi-model predictions confirm previous findings reported in AR4 (e.g. Kuzmina, 2005; Stephenson et al., 2006), of a positive trend in future winter NAO (Gillett and Fyfe, 2013; Karpechko, 2010). However, there are substantial variations between NAO projections from different climate models. For example, Fischer-Bruns

et al. (2008) have employed an atmosphere–ocean coupled model (ECHAM4-OPYC3) and used the empirical orthogonal function (EOF) analysis to investigate future trends in the NAO. The study found no detectable shift in the leading mode of atmospheric variability under global warming scenarios. On the other hand, Müller and Roeckner (2008) found a strong positive trend in the NAO in the ECHAM5/MPI-OM simulations. As a consequence of such uncertainties, the IPCC AR5 has expressed only medium confidence in near-term projections of NAO changes (IPCC, 2013).

Recently, atmospheric variability in the North Atlantic and the NAO pattern have also been linked to Rossby wave-breaking in the upper troposphere and to atmospheric blocking (e.g. Croci-Maspoli et al., 2007; Woollings et al., 2008). The term *atmospheric blocking* is broadly used to describe situations in which the prevailing westerly flow is blocked, or distorted by a persistent, quasi-stationary anticyclone (e.g. Rex, 1950; Berrisford et al., 2007). However, the exact definition varies among studies. For example, Pelly and Hoskins (2003) pioneered the use of potential vorticity (PV) as an indicator for blocking, linking blocking occurrences to the meridional potential temperature gradient on a constant PV surface. In this framework, atmospheric blocking is therefore associated with Rossby wave breaking. It has been shown that different blocking patterns correspond to significantly different large-scale atmospheric circulations over the North Atlantic Basin (Rex, 1950). Blocking situations are often responsible for stagnant atmospheric conditions that lead to the accumulation of pollutants at ground levels. This increases the likelihood of exceeding particulate matter (PM) annual and daily limit concentrations, such as those imposed by European regulations (Directive 2008/50/EC).

The aim of this paper is to disentangle the role of future aerosol and GHG concentration changes in altering atmospheric circulation, expanding earlier analysis that focussed on global scale climate impacts (Kloster et al., 2009) and the relationship between air pollution mitigation and extreme events (Kloster et al., 2009; Sillmann et al., 2013). We focus on the extreme case that by 2030 aerosol concentrations will be globally reduced to the maximum feasible extent by using all presently available end-of-pipe technology, using the results of an aerosol–atmosphere model coupled with a mixed-layer ocean. Finally, we evaluate the impact of such atmospheric circulation changes onto PM variability. The analysis includes simulations in which only GHG concentrations, only aerosol emissions, or both, are changed. In each simulation the anthropogenic emission scenarios used to force the model are constant for the entire length of the integration; hence, the changes in variability depicted by the model will be associated with changes in atmospheric circulation only. We investigate how GHG and/or aerosol forcings act on: (i) the structure of the SLP meridional dipole over the North Atlantic in terms of strength and location of its centres of action; (ii) changes in the NAO in the near future; (iii) the spatial structure and frequency of atmospheric blocking in

the North Atlantic. Finally, we also examine (iv) how future changes in atmospheric circulation could impact air quality over Europe.

This work is structured as follows: Sect. 2 describes the model used, the simulation set-up and the statistical tools adopted; Sect. 3 presents the GHG and aerosol-induced changes in the magnitude and spatial pattern of the meridional SLP dipole in the North Atlantic. We also discuss the related changes in the NAO and atmospheric blocking over the Atlantic, and the effects of such changes on PM variability. Discussions and conclusions are presented in Sect. 4.

2 Methods

2.1 Climate model

We have analysed the climate simulations performed by Kloster et al. (2008, 2009) using the ECHAM5-HAM aerosol–climate model. We focus on the analysis of hitherto unexplored aspects of atmospheric circulation changes over the North Atlantic. These simulations were also used by Sillmann et al. (2013) to analyse how future changes on aerosol concentrations impact on precipitation; however, they focused on annual means and did not consider to what extent these changes were reflected by large-scale circulation changes that were driving the more localized precipitation responses.

The ECHAM5-HAM modelling system includes the atmospheric general circulation model ECHAM5 (Roeckner et al., 2003) coupled to a mixed layer ocean (Roeckner et al., 1995), and the microphysical aerosol model HAM (Stier et al., 2005). The ECHAM5-HAM simulations analysed in this study (Kloster et al., 2008, 2009) account for both the direct and indirect (cloud lifetime and cloud albedo effect) aerosol effects. ECHAM5 was run on a T63 horizontal grid (about 1.8° on a Gaussian grid), and on 31 vertical levels from the surface up to 10 hPa. A cloud scheme with a prognostic treatment of cloud droplet and ice crystal number concentration (Lohmann et al., 2007) provided fractional cloud cover prediction from relative humidity (Sundquist et al., 1989). The shortwave radiation scheme included six bands in the visible and ultraviolet spectra (Cagnazzo et al., 2007).

The microphysical aerosol module HAM treats the aerosol size distribution, mixing state and composition as prognostic variables. It predicts the evolution of an ensemble of interacting aerosol modes and is composed of the microphysical core M7 (Vignati et al., 2004); an emission module for SO_2, black and organic carbon, and mineral dust particles; a sulphur oxidation chemistry scheme using prescribed oxidant concentrations for OH, NO_2, O_3 and H_2O_2 (Feichter et al., 1996); a deposition module; and a module defining the aerosol radiative properties. Prescribing oxidant concentrations, most importantly H_2O_2, may have led to an underestimate in the resulting sulfate burden, since the use of off-line H_2O_2 may not

accurately account for depletion by aqueous reactions with SO_2 and recovery in cloud-free conditions. This will increase the gas-phase production of SO_4 which is less susceptible to scavenging, and increase the SO_4 burden (Barth et al., 2000; Roelofs et al., 1998). Another model evaluation of the effect of including explicit oxidation (Pham, 2005) suggested an overall decline of SO_4 burden ($< 1\%$), but an increase of SO_4 surface concentrations (ca. 5 % in many regions), due to a combination of increased near-surface oxidation and removal processes. This is a relatively minor error compared to other uncertainties (Textor et al., 2007). The aerosol optical properties were explicitly simulated using Mie theory and provided as input for the radiation scheme in ECHAM5 following Toon and Ackerman (1981). Climate-sensitive natural emissions (dimethyl sulphide, sea salt and dust) were simulated interactively.

2.2 Simulation set-up

The GHG concentrations used in the simulations were derived from the IMAGE 2.2 implementation of the SRES B2 scenario (IMAGE-team, 2001). The SRES B2 storyline describes a world with intermediate population and economic growth, in which the emphasis is on local solutions to economic, social and environmental sustainability.

The anthropogenic emissions of carbonaceous aerosols, namely black carbon (BC) and organic carbon (OC), as well as sulphur dioxide (SO_2), the main precursor of sulphate aerosols, are extracted from an aerosol emission inventory developed by the International Institute for Applied System Analysis (IIASA). In this work, a maximum feasible reduction (MFR) air pollutant emission scenario was explored for the year 2030 (Cofala et al., 2007). MFR assumes the full implementation of the most advanced available technologies for aerosol emissions abatement. It is built using projections of human activity levels (industrial production, fuel consumption, livestock numbers, crop farming, waste treatment and disposal) based on current national perspectives on the economic and energy development up to the year 2030. In regions where data were not available, the economic and energy future trends estimated in the IPCC SRES B2 MESSAGE scenario (Nakicenovic et al., 2000; Riahi and Roehrl, 2000) were considered. Biomass burning emissions, both anthropogenic and natural, were assumed to stay constant at 2000 levels. Changes in land use were not taken into account.

In the present study, the modifications of future North Atlantic atmospheric circulation are assessed by analysing the differences between near future (year 2030) and present-day (year 2000) conditions reproduced in climate equilibrium simulations. A 60-year control simulation was performed with GHG concentrations, aerosol and aerosol precursor emissions of the year 2000, and three 30-year sensitivity equilibrium experiments were performed, using three different combinations of GHG concentrations and aerosol emissions scenarios:

– 2000 experiment: year 2000 GHG concentrations and aerosol emissions;

– 2030 experiment: year 2030 GHG concentrations and MFR aerosol emission scenario;

– 2030GHG experiment: year 2030 GHG concentrations, and 2000 aerosol emissions;

– 2030AER experiment: year 2000 GHG concentrations, and 2030 MFR aerosol emission scenario.

All simulations used a spin-up of 30 years, not included in the analysis.

The 2030GHG and 2030AER experiments in which, respectively, aerosol emissions and GHG concentrations remained at the 2000 level, were performed to separate the effects of GHG concentrations and aerosols emissions. The experimental setups are summarized in Table 1.

2.3 Statistical analysis methods

We evaluate three aspects of the large-scale circulation: (1) the SLP spatial structure (shift of centres of action); (2) the leading mode of atmospheric variability (NAO); and (3) the blocking frequency. Finally, we investigate how the atmospheric circulation changes affect PM distributions.

To investigate the impact of aerosol and GHG concentration changes on SLP spatial structure, we define the SLP centres of action for the winter season (December, January and February, DJF) by creating SLP coherence maps (Pausata et al. 2009). The coherence index value ($0 \leq CI \leq 1$) at each grid-point is the absolute value of the area-averaged correlation between the monthly SLP time series at that point and over the rest of the North Atlantic Basin (20–85° N; 90° W–40° E). Higher values indicate that the SLP variability at that location is more *coherent* with variability throughout the North Atlantic, either in-phase or anti-phase. The Northern and Southern SLP Centres Of Action (NCOA and SCOA) are identified as CI maxima over the North (north of 55° N) and subtropical Atlantic (south of 55° N), respectively. This method allows determining the spatial distribution and shifts of the COAs due to aerosol and GHG concentration changes, both in combination and separately (for details see Appendix A). In order to verify that the computed geographical shifts in the centres of action are outside the normal range of inter-annual variability, we use a statistical bootstrap approach to produce a set of 100 CI maps for the 2000 experiment. We randomly select subsamples of 20 years for the 30-year-long simulations and subsamples of 40 years for the 2000 (60-year-long) simulation, and perform the CI analysis for each subsample. Subsequently, we apply the Student's t test to determine whether the CI pattern and the shift in the centres of action between the 2000 control simulation and the sensitivity studies are significant at 95 % confidence level.

Table 1. ECHAM5-HAM experiment design and number of years simulated for each experiment. The original denomination used by Kloster et al. (2009) is shown in the last column.

Experiment	GHG	Aerosol emissions	Years of simulation	Original names
2000	2000	2000	60	CONTROL
2030	2030	2030	30	GHG + AE
2030GHG	2030	2000	30	GHG
2030AER	2000	2030	30	AE

Furthermore, in order to assess the variability of the SCOA and evaluate its relation to blocking frequency and precipitation in the 2000 simulations, we construct an index of the SCOA (SCOAI). We first generate 10 000 random subsamples of 15 years from the 60-year pool of the 2000 simulation. In this case we have reduced the subsample size from 40 to 15 years in order to increase the variability of the SCOA and hence, better understand its influence on blocking frequency and precipitation. We then calculate the CI values and determine the position of the SCOA (maximum in the CI south of 55° N) for each subsample. Hence, we construct the SCOAI where the value of 0 is defined as the 50th percentile of the SCOA position within the 10 000 subsamples. Eastward positions (relative to the 50th percentile) of the SCOA are defined as positive values of the SCOAI and westward position as negative ones. The SCAOI is then normalized by the standard deviations of the eastward and westward SCOA positions.

Winter changes in the leading mode of atmospheric variability are investigated by using the monthly NAO Index (NAOI), defined as the difference in the normalized SLP anomalies between Ponta Delgada, Azores, and Stykkishólmur/Reykjavik, Iceland. The NAOI allows one to look for shifts in the North Atlantic atmospheric circulation associated with future climate change (Hurrell, 1995).

The analysis of blocking frequency over the North Atlantic Basin is performed as follows. In order to define atmospheric blocking, the present paper utilizes a bi-dimensional index that identifies reversals in the meridional gradient of 500 hPa geopotential height (Davini and Cagnazzo, 2013; Davini et al., 2012; Tibaldi and Molteni, 1990). For every model grid-box with coordinates (latitude $= \varphi$, longitude $= \lambda$), the following two quantities are defined:

$$\Delta_N(\varphi\lambda) = \frac{Z_{500}(\varphi, \lambda) - Z_{500}(\varphi - 15°, \lambda)}{15°}, \quad (1)$$

$$\Delta_S(\varphi\lambda) = \frac{Z_{500}(\varphi + 15°, \lambda) - Z_{500}(\varphi, \lambda)}{15°}, \quad (2)$$

over the domain where:

30°N $< \varphi <$ 72.5°N, 180°W $< \lambda \leq$ 180°E.

In order for a gridbox to be flagged as "blocked", the following must hold:

$$\Delta_N > 0; \; \Delta_S < -10 \, \text{m} / (^\circ \text{latitude}).$$

In order to define a blocking event, a number of additional constraints are also enforced. Firstly, a cluster of adjacent blocked gridboxes spanning at least 15° longitude must be identified at a given time step. Therefore, if a gridbox is blocked in isolation, it is not considered to be part of a blocking event. A persistence criterion is also applied: a blocking event requires that at least one other blocked gridbox is detected for 5 consecutive days within an area of 5° latitude by 10° longitude, centred on the original blocked gridbox.

The impacts of changes in atmospheric circulation on air pollution are investigated by analysing changes in PM monthly anomaly distributions. We focus on changes in the skewness of distributions for the winter season. The skewness is the distribution's third standardized moment, and is a measure of the asymmetry of the distribution. Positive skewness values typically indicate that the right side tail of the distribution becomes longer than the left side, and vice versa for negative values. Significance in the skewness differences is assessed by using a Kolmogorov–Smirnov test at 95 % confidence level. This test is a non-parametric tool, meaning that it makes no assumptions on the shape of the data distribution. An "artificial" variability is introduced in the skewness values in each simulation through a bootstrap technique. For each experiment, we calculate the skewness values of 100 random distributions, generated from the original pool of 30 or 60 years using the same bootstrap technique described for the CI. The significance level is then identified based on this sample.

3 Results

The results presented here describe the effects of GHG and aerosol concentrations on the mean state and variability of the North Atlantic atmospheric circulation. The results are presented in three sections. In the first section, changes in the spatial structure of the SLP and its variability are investigated. In the second section, we extend the analysis to changes in the blocking frequency. Finally, in the third section, we quantify the impacts of such changes on precipitation regime and PM variability.

3.1 Changes in SLP centres of action and their variability

The 2030 and 2030AER simulations show a north-eastward shift of the SCOA compared to the 2000 control simulation (Fig. 1). The area of highest SLP coherence in the 2000 simulation is located in the central-western part of the sub-tropical North Atlantic, whereas in the 2030 simulation it is shifted off the coast of northern Morocco. The NCOA, instead, re-

mains located in central-western Greenland for all scenarios. However, in the 2030 and 2030AER simulations, a secondary CI maximum develops in the Norwegian Sea, and the areas with the CI maxima are broader. Secondary CI maxima also develop at low latitudes compared to the 2000 simulation (Fig. 1).

Both sensitivity simulations (2030GHG and 2030AER) show a significant north-eastward shift (see Sect. 2.3) of the SCOA as well as broader areas of CI maxima compared to the 2000 simulation. Both these features are more pronounced in the 2030AER than in the 2030GHG simulation, in particular the displacement towards the Mediterranean Sea of the SCOA.

With regard to the SLP variability, the 2030 simulation shows a significant positive shift of the NAO mean state by 0.46 compared to the 2000 control period (Fig. 2). The probability of having an NAOI greater than $+1$ increases from 30 to 40 %. (Fig. 2). Neither the GHG increase (2030GHG) nor the aerosol reduction (2030AER) have any statistically significant role in changing the NAO mean state and the frequency distribution of strongly positive/negative NAO phases relative to the control simulation. Nevertheless, the GHG increase is more likely to contribute to the NAO shift compared to aerosol alone: in the 2030AER simulation the null hypothesis that aerosols do not affect the NAO can be excluded with a likelihood of 65 %, while in the 2030GHG simulation the same likelihood is 85 % (using a t test). Only the combination of both 2030 GHGs and aerosol emissions leads to a statistically significant change in the NAO mean state at 95 % confidence level.

Hence, whereas the NAO shift is related to both aerosol and GHG changes (with likely stronger impacts from the GHGs), the aerosol reduction alone plays the largest role in shifting the southern centre of action of SLP towards the Mediterranean.

3.2 Changes in blocking frequency

Blocking events can have a large impact on weather patterns and sometimes lead to the occurrence of extreme events (e.g. Yiou and Nogaj, 2004); hence, it is important to quantify the variability and possible changes in the preferred location of blocking occurrences.

The 2000 simulation shows a blocking frequency that peaks in the south over the sub-tropical North Atlantic (low-latitude blocking, LLB) and in the north over Greenland (high-latitude blocking, HLB), as shown in Fig. 3a. The LLB events are linked to a northward displacement of the sub-tropical high-pressure system. The HLB events are characterized by long durations (on the order of 9 days), diverting the main flow southward (Davini et al., 2012). The simulated 2000 blocking climatology is slightly different from the patterns seen in re-analysis data, which have a higher activity over the Nordic seas, but nevertheless shows a strong resem-

blance to the observed climatology (cf. Fig. 3a with Fig. 1 in Davini et al., 2012).

HLBs and LLBs are strongly tied to the phase of the NAO: Woollings et al. (2008) showed that HLB events over Greenland are strongly anti-correlated with the NAOI. Furthermore, changes in the HLB position (Wang and Magnusdottir, 2012) and frequency (Davini et al., 2013) have been shown to influence not only the NAOI, but also its pattern. Yao and Luo (2014) have described the relationship between HLBs and LLBs and the NAO phase in winter during the period 1950–2011. The HLBs are connected not only to the NAO phase but also to the position of the SCOA. By regressing the NAOI and the SCOAI time series onto the blocking frequency field in the 2000 simulation (see details in Appendix B), we analyse how the NAO phase and the position of the SCOA affect the blocking frequency. Positive NAO phases are associated to a northward increase of LLBs (Fig. 4a), whereas eastward positions of the SCOA are connected to a north-eastward increase of LLBs (Fig. 4b). The regression analysis also shows a decreased HLB frequency over Greenland during positive NAO phases in agreement with the above-mentioned studies.

The 2030 simulation shows a significant increase (up to 50–70 %) in the number of LLB events over western Europe and the Mediterranean Basin, corresponding to a more invasive subtropical anticyclone (high-pressure system) over southern and central Europe in winter. The increased LLB frequency in the 2030 simulation is consistent with both a positive NAO shift (Fig. 4a) and an eastward shift of the SCOA (Fig. 4b). On the other hand, HLBs decrease (Fig. 3b) is in agreement with the reduction in negative NAO phases discussed in Sect. 3.1 and the NAOI-blocking frequency relationship highlighted in Fig. 4a.

The 2030GHG and 2030AER simulations also show significant increases in the LLB frequency over the mid-latitude North Atlantic and decreases in the HLB frequency (Fig. 3c, d). However, the patterns are different from one another: the high-latitude change in both 2030GHG and 2030 closely approximates the blocking frequency difference between the positive and negative phases of the NAO, shown in Fig. 4a (cf. with Fig. 3b, c). On the other hand, the HLB frequency change in the 2030AER experiment seems to be related to a shift in the SCOA (cf. Figs. 3d and 4b). This is consistent with the large (small) eastward displacement of the SCOA in the 2030AER (2030GHG) simulation and the smaller (larger) shift in the NAO mean state.

The 2030AER simulation also shows a significant increase in LLB frequency over the Mediterranean, not seen in the 2030GHG experiment. Hence, the aerosol concentration reduction seems to be the main driver of the increase in LLB events over the Mediterranean seen in the 2030 simulation (Fig. 3 cf. panels b and d). These results strengthen the role of aerosols in affecting atmospheric dynamics in the North Atlantic, suggesting that they drive both (a) an eastward shift of the southern centre of action of SLP and (b) an increased

tendency of the sub-tropical anticyclone to expand towards the Mediterranean Sea.

3.3 Impacts on air quality

Large-scale changes in atmospheric circulation can affect PM variability over Europe by altering the precipitation regime. The latter is one of the main mechanisms for PM removal, and affects PM concentrations at the surface (e.g. Horton et al., 2014; Jacob and Winner, 2009; Pausata et al., 2013). For example, an eastward shift of the SCOA and/or a shift towards positive NAOI, together with an increased frequency of blocking events in the Mediterranean, may lead to a higher frequency of dry, stagnant weather conditions in south-western Europe, thus worsening air quality (see Appendix C for a discussion on the relationship between circulation changes and precipitation). Hence, even though there will be an overall improvement in air-quality conditions associated with an abatement of PM emissions, additional PM emission reduction measures may be necessary for those countries and cities lying in the Mediterranean area, to counterbalance the effects of the atmospheric circulation changes. This hypothesis has already been suggested by Pausata et al. (2013) on the basis of an NAO-PM analysis using the same model driven by ERA-40 re-analysis data. In this work, we test it further by analysing climate sensitivity experiments under different aerosol emission scenarios for the near future. We aim to provide a general coherent overview of the impacts of large-scale circulation changes on air quality. We focus on monthly PM data, similar to the monthly SLP field used for the NAOI and CI analyses. We do not discuss the daily exceedances of EU thresholds, since this would be beyond the scope of the present study, and the coarse resolution global model has limited skills for simulating them (Pausata et al., 2013).

To quantify how the changes in atmospheric circulation affect air quality, we calculate the relative anomaly distributions of PM concentrations for four regions (see also Fig. 3a), to encompass the different areas of influence of the NAO over Europe:

- Western Mediterranean (WM): 34–43° N/0–10° W;

- Eastern Mediterranean (EM): 34–43° N/10–40° E;

- Central Europe (CE): 44–53° N/0–15° E;

- Eastern Europe (EE): 46–60° N/20–40° E.

In the PM we have considered only the aerosol components included in ECHAM5-HAM that have a predominantly anthropogenic signature – namely black and organic carbon, and sulphates – disregarding aerosols of natural origin (e.g. sea-salt, mineral dust). Thus, the PM in this paper represents mostly $PM_{2.5}$, and is likely a lower bound on the "real" PM concentrations (for an evaluation of correspondence between
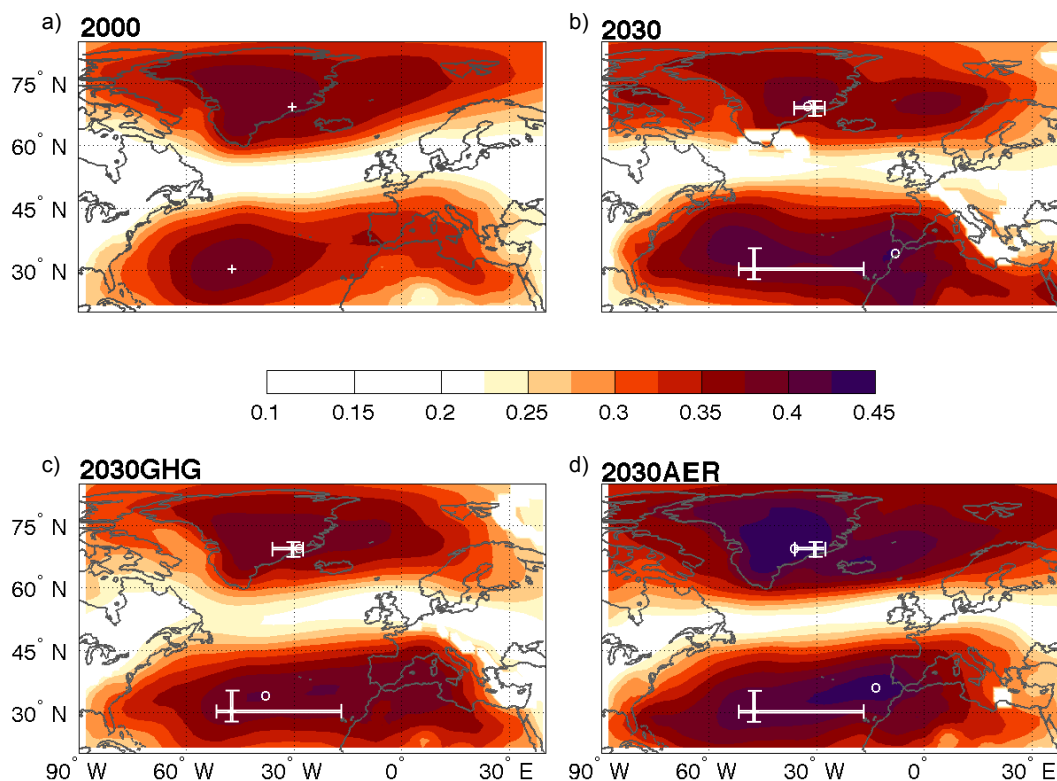
Figure 1. Sea-level pressure coherence index maps of the North Atlantic sector for the 2000 (**a**) and 2030 (**b**) simulations and the two sensitivity studies (**c**, **d**) in winter (DJF). The SLP centres of action (COAs) for the control run and for the 2030 simulations are shown by white crosses and white circles, respectively. The bars delimit the range between the 10th and 90th percentile of the CI maxima in the 2000 simulations. Only areas in which the difference between the 2000 control pattern and the sensitivity simulation is significant at the 95 % confidence level and CI values are greater than 0.225 are shaded. The choice of shading only CI values greater than 0.225 is arbitrary.

modelled and measured $PM_{2.5} / PM_{10}$ see the Supplementary Material in Pausata et al., 2013).

First, we analyse the skewnesses of the monthly PM relative anomaly distributions for the winter season. PM relative anomaly distributions for all experiments and for all four regions show positive skewness values, meaning that positive PM anomalies are becoming more likely than negative ones (Fig. 5 and Table 2). Our results show that, in all three 2030 experiments, the simulated PM distributions change significantly in all regions considered due to the altered atmospheric circulation (Fig. 5 and Table 2).

In the Western Mediterranean (WM), the PM relative anomaly skewness increases remarkably from 0.26 in the 2000 case to 1.02 and 1.05 in the 2030 and 2030AER simulations, respectively. This change is mainly led by the aerosol reduction, whereas the GHGs only drive a small contribution (Table 2). The large change in skewness in the 2030 simulation is accompanied by a corresponding shift in the upper and lower percentiles of the distribution. The 5th and 95th percentiles rise by 8 and 4 % respectively relative to 2000, indicating a transition towards more positive PM anomalies (Table 3). The rise in PM extremes matches the changes in rainy day extreme percentiles (not shown). The 95th and 5th

Table 2. Skewness values for the PM distributions of the four selected regions for each experiment. For each region and experiment, changes relative to all the other experiments are significant at the 95 % confidence level, except for 2030-2030AER in Western Mediterranean.

	Western Mediterranean	Eastern Mediterranean	Central Europe	Eastern Europe
2000	0.26	0.83	1.44	1.70
2030	1.02	0.95	0.66	1.18
2030GHG	0.48	1.26	1.18	1.08
2030AER	1.05	1.17	0.94	1.03

percentiles of the frequency of rainy days decrease by 2 and 17 % respectively. Rainy day frequencies and PM anomalies are anti-correlated; therefore, a change in the 95th (5th) percentile in rainy days should be associated with a change of the opposite sign in the 5th (95th) percentile in the PM anomalies.

The Eastern Mediterranean (EM) also experiences an increased skewness in the 2030 simulation relative to 2000. However, the changes are smaller compared to the WM, possibly because of the greater distance from the SCOA – lo-
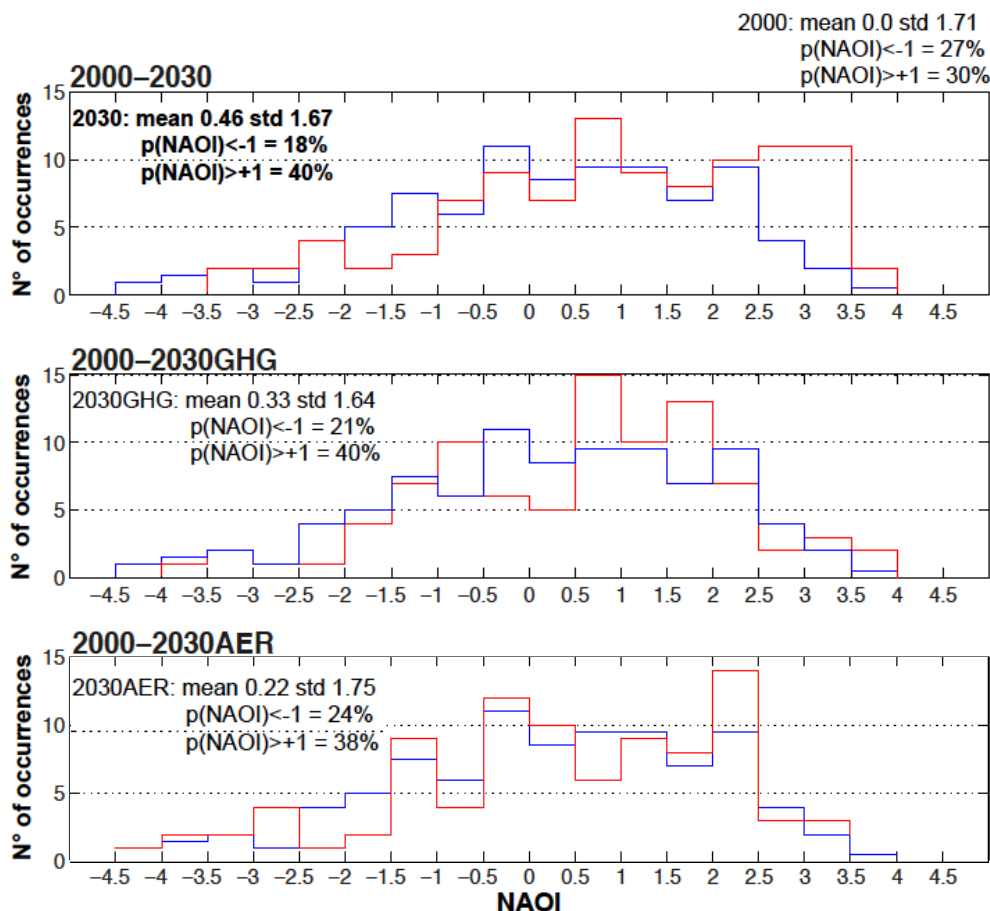
Figure 2. Frequency distributions of the winter (DJF) NAOI for the 2000 control simulation (blue, all panels), 2030 (red, upper panel), 2030GHG (red, central panel) and 2030AER (red, lower panel). Numbers show the NAOI mean value, the standard deviation (SD) and the probability of having a NAOI greater than $+1$ ($p(\mathrm{NAOI}) > +1$) or smaller than -1 ($p(\mathrm{NAOI}) < -1$). Values of the simulations having a NAOI mean significantly different from 2000 control mean at 95 % confidence level are shown in bold. The 2000s mean NAO is by definition equal to 0 and the number of occurrences has been normalized to 30 years for a direct comparison with the other simulations.

Table 3. PM relative anomalies (unitless) associated to different percentiles for the WM and CE regions in the 2000 experiment (first and third rows) and their relative changes (in %) for the 2030 simulation compared to 2000 values (second and fourth rows).

| Region	Experiment	Percentile				
		5th	25th	50th	75th	95th
Western Mediterranean	2000	0.49	0.73	1.01	1.25	1.57
	2030	+8 %	+1 %	−9 %	−7 %	+4 %
Central Europe	2000	0.65	0.80	0.94	1.13	1.48
	2030	−14 %	−3 %	+2 %	+2 %	+7 %

cated off the coast of the Iberian Peninsula in the 2030 simulation – and the contrasting effect of the NAO phase inside the domain: as one moves further to the east in the Mediterranean Basin, the correlation between NAO and precipitation changes sign (Fig. B1a). The smaller changes in the PM distribution simulated in the EM compared to the WM could therefore be related to a different behaviour in precipitation regime (see Appendix B).

On the other hand, Central (CE) and Eastern Europe (EE) show a decreased skewness in the 2030 case compared to the 2000 simulation. CE displays a shift in skewness from 1.44 to 0.66; the corresponding shift in EE is from 1.70 to 1.18. Furthermore, CE also shows an increment in the number of negative extremes, with a 14 % decrease in the 5th percentile. However, CE also experiences an increase in positive extremes with a +7 % shift in the 95th percentile in the 2030
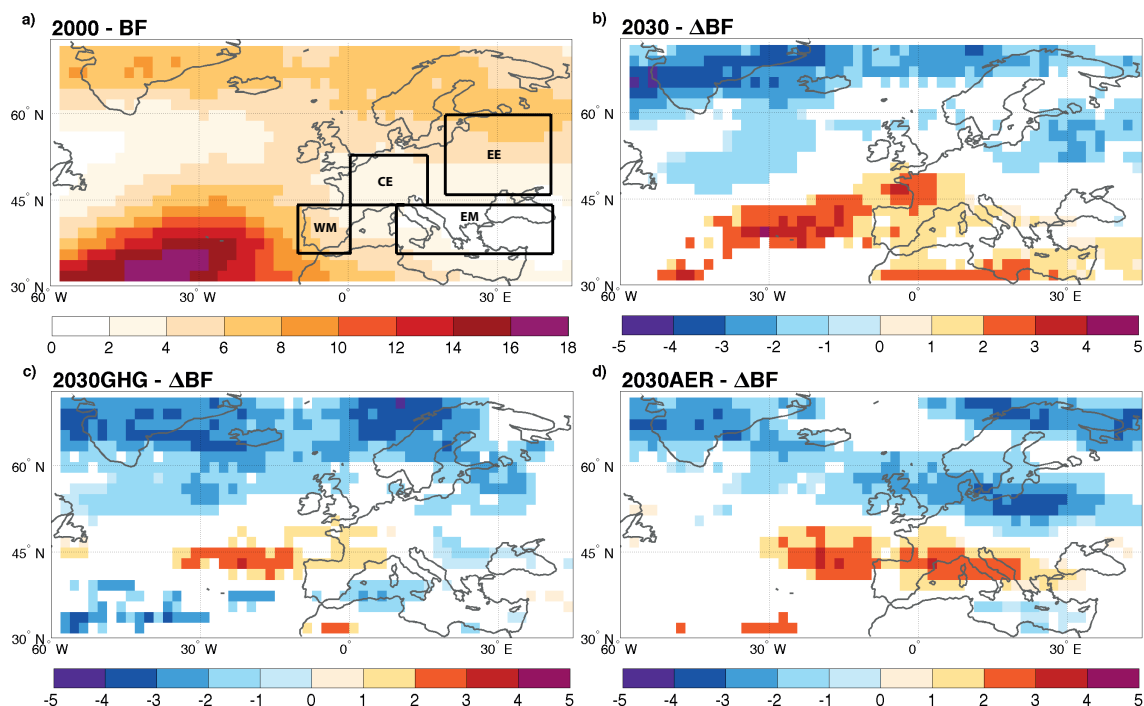
Figure 3. Blocking frequency (in % of days in which a blocking event occurs at a given gridbox) over the Atlantic sector for the 2000 simulation (**a**); changes in blocking frequency compared to the 2000 simulation for 2030 (**b**), 2030GHG (**c**) and 2030AER (**d**) simulations in winter (DJF). Only areas in which the difference between the 2000 control and the sensitivity simulation is significant at 95 % confidence level are shaded (in white non-significant areas). In panel (**a**) we have highlighted the regions discussed in Sect. 3.3 and Table 2.
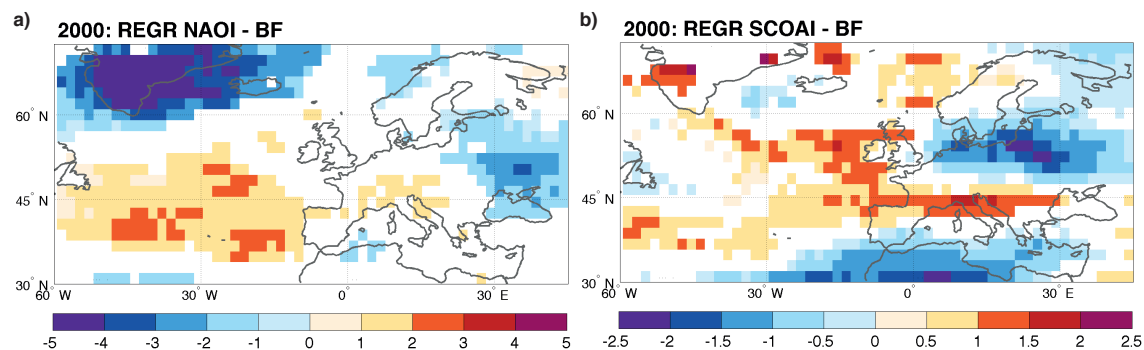

Figure 4. Blocking frequency anomalies (in % of days in which a blocking event occurs at a given gridbox) per unit of NAO index (NAOI, **a**) and SCOA index (SCOAI, **b**) standard deviation. The anomalies are calculated using a one-point regression analysis (see Appendix B). Only differences significant at 95 % confidence level are shown (based on the correlation significance between NAOI/SCOAI and blocking frequency). Note that the two panels use different colour scales.

simulation compared to the 2000 experiment (Table 3). The change in the extreme PM percentiles is accompanied by a similar but opposite change in the rainy day percentiles: +3 and −9 % for the 95th and 5th percentiles, respectively. CE is located closer to the transition area of the NAO influence between northern Europe and Mediterranean Basin (see also Fig. B1). Therefore, this area may be exposed to alternation of a more invasive Azores high and rainy Atlantic storms.

Therefore, the regions that will be most affected by future large-scale circulation changes are the Western Mediter-ranean and Central Europe, both with increased high PM concentration episodes, but the latter also with a strong increment in low PM values relative to 2000. The implications of these results for air-quality policy are discussed in the following section.
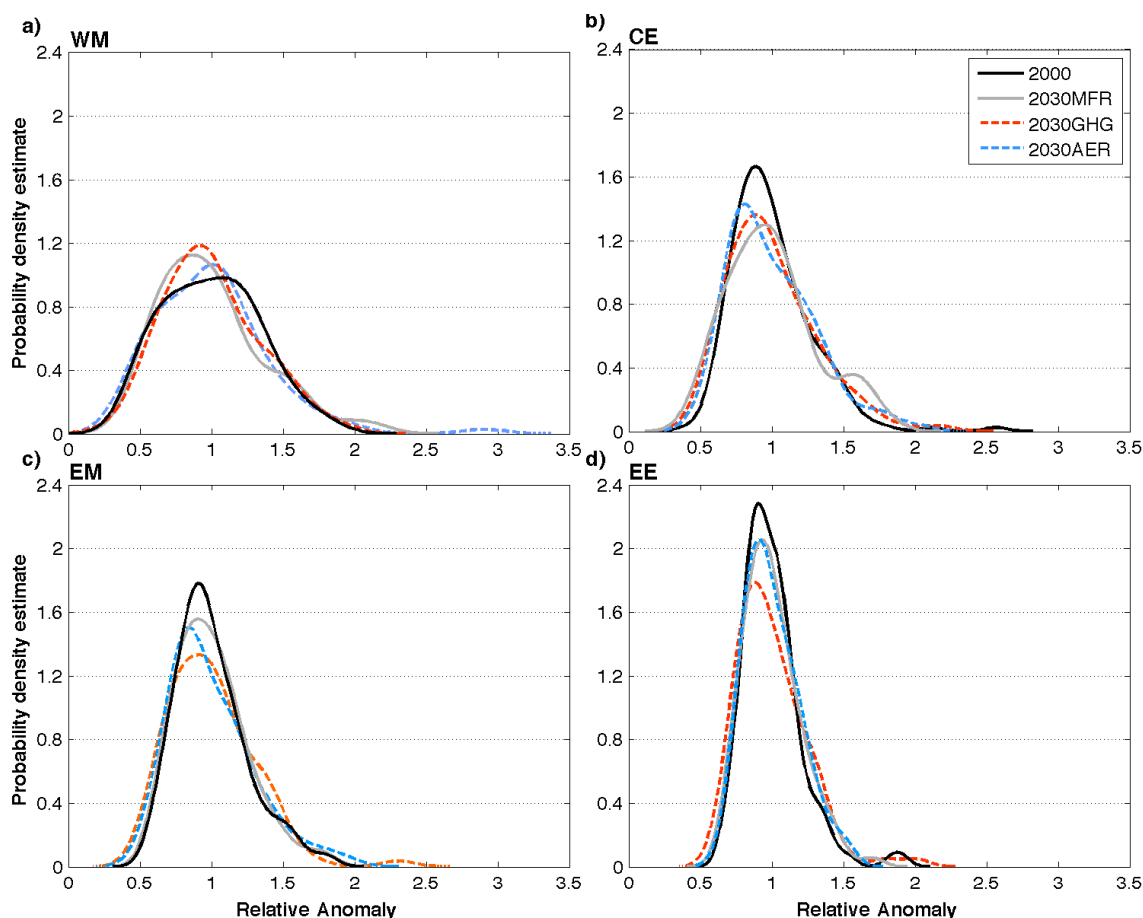
Figure 5. Probability density estimates (PDEs) of PM relative anomalies for each region (Western **(a)** and Eastern Mediterranean **(c)**, Central **(b)** and Eastern Europe **(d)**)) and for each experiment. Relative anomalies are computed as the ratio between winter (DJF) monthly time series and the winter (DJF) climatology of each experiment and region. The probability density estimates are based on a normal kernel function, which provides non-parametric PDEs for random variables (Rosenblatt, 1956). The probability for a given relative anomaly to occur is obtained by integrating the PDE in dx.

4 Discussion and conclusions

The present study analyses future scenarios of atmospheric circulation over the North Atlantic and possible impacts on air quality over Europe. The chemistry–atmosphere ECHAM5-HAM model, coupled to a mixed layer ocean, shows a change towards more positive NAO phases, together with an eastward shift of the southern SLP centre of action. These shifts are associated with an increased frequency of blocking events over the western Mediterranean. Our results highlight how the decreased aerosol and aerosol precursor emissions, along with GHGs, are responsible for changes in radiative forcing that feedback onto the atmospheric circulation and alter the NAO mean state. Table 4 provides a qualitative summary of the atmospheric changes induced by 2030 GHGs, aerosols and jointly by GHG and aerosol emissions on a variety of circulation indicators. These changes in atmospheric circulation in turn feedback significantly on air quality, and would lead to an increase in the magnitude of extreme pollution events over the western Mediterranean if no changes in aerosol emissions were observed. In the MFR scenario analysed in our study, however, the reduction in aerosol emissions would outstand the increase in PM extreme values leading to an overall improvement of air quality.

Future shifts in the NAO phase have already been discussed by several modelling studies (e.g. Gillett and Fyfe, 2013; Karpechko, 2010; Stephenson et al., 2006; Kuzmina, 2005; Hu and Wu, 2004); however, the driving mechanisms behind these shifts are still under debate. Hori et al. (2007) have shown that NAO variability does not change substantially in the SRES-A1B scenarios compared to the 20th century, and conclude that the trend in the NAO index is the result of an anthropogenic trend in the basic mean state, rather than being due to changes in NAO variability. Our results support the findings of Hori et al. (2007) by showing that anthropogenic changes in GHG and aerosols lead to a change in the NAO's mean state rather than its variability (Fig. 2).

Table 4. Qualitative contributions (small (+), medium (++), high (+++)) of 2030GHG and 2030AER to changes in the NAO phase, SCOA location and blocking event frequency. For the blocking events, the direction of the increased frequency is also shown. The contributions significant at 95 % confidence level are shown in bold.

	Impact on NAO	Impact on SCOA	Impact on blocking events
2030GHG	++	+	**North ++** **East+**
2030AER	+	+++	**North ++** **East +++**
2030 (GHG+AER)	+++	+++	**North +++** **East +++**

The positive NAO shift comes along with a shift of the SLP centres of action. Hilmer and Jung (2000) have found an eastward shift in the SLP pattern associated with the inter-annual variability of the NAO from 1958–1977 to 1978–1997. Peterson et al. (2003) have suggested that this shift is simply a consequence of the trend towards a more positive NAO index in the last two decades of the 20th century. Hu and Wu (2004), using both data and a coupled general circulation model, have also shown that a shift of both SLP centres of action took place in the second half of the last century, which will likely continue in the future. Our study confirms that this shift also occurs under a global warming scenario. However, while in our simulations the southern centre undergoes a remarkable eastward shift, the northern one is fairly stable around southern Greenland – as demonstrated using the coherence index approach (Fig. 1). Nevertheless, the CI maps do show that in the 2030 simulations a secondary northern maximum – not present in the 2000 experiment – appears in the Norwegian Sea (Fig. 1). Furthermore, our simulations highlight how the future abatement of the aerosol load may play an important role in the eastward shift of the SLP centres of action.

The present study also finds an increased blocking frequency over the western Mediterranean. Such an increase, together with an eastward displacement of the southern SLP centre of action and a positive shift of the NAO mean state, leads to more frequent stagnant weather conditions that favour pollutant accumulation in the Mediterranean. This change in frequency of pollution events has also been described by Kloster et al. (2009), who showed that aerosol abundance is dependent on the climate state, as also highlighted in a number of other modelling studies (e.g. Feichter et al., 2004; and overview in IPCC, 2013). Kloster et al. (2009) further found that aerosol burdens increase in the area due to less precipitation and reduced wet deposition. Hence, they suggest that climate change alone would worsen air pollution by aerosols. Here we show that in Europe these findings are consistent with a straightforward NAO-behaviour analysis. A positive shift in future NAO would indeed lead to more intense extreme pollution events over

specific areas, such as the western Mediterranean countries, assuming constant present-day aerosol emissions. This result also supports the hypothesis of Pausata et al. (2013) that – for aerosol emissions fixed at present day values – climate change would lead to more extreme pollution events over the western Mediterranean, forcing southern European countries to implement more stringent abatement measures to counteract adverse changes in PM variability. However, our study also highlights that the increase in the number of high PM episodes in the western Mediterranean is partially counterbalanced by a lower median and a narrowing of the PM frequency distribution around the median itself (Fig. 5 and Table 3).

Current European legislation considers PM air-quality thresholds of $25\,\mu g\,m^{-3}$ (annual average) for $PM_{2.5}$, and $50\,\mu g\,m^{-3}$ for PM_{10} (daily average, not to be exceeded for more than 35 days per year). European legislation has also set an indicative target value of $20\,\mu g\,m^{-3}$ for the $PM_{2.5}$ annual average. Currently, between 20–31 % and 22–33 % of the urban population in Europe is exposed to $PM_{2.5}$ levels above the $20\,\mu g\,m^{-3}$ threshold (EEA, 2013). However, more stringent standards are currently in place in the USA (annual $PM_{2.5}$: $12\,\mu g\,m^{-3}$), and are recommended by the World Health Organization – WHO (annual $PM_{2.5}$ / PM_{10}: $10/20\,\mu g\,m^{-3}$), and may be adopted in Europe as well at some point in the future. Considering the more stringent WHO guidelines, currently between 91–96 % ($PM_{2.5}$) and 85–88 % (PM_{10}) of the urban population is exposed to values above the thresholds (http://ec.europa.eu/environment/air/quality/standards.htm). Depending on threshold levels set by future EU air-quality legislation, it is not a priori clear how changes in PM frequency distributions will affect exceedance of these thresholds, and what levels of emission reductions are appropriate to reach these air-quality objectives.

Unfortunately, our coarse resolution global model results only allow a qualitative assessment of the impact on air quality exceedance of future air pollution emissions and climate change. Therefore, we envision the need for more in-depth studies to further quantify the significance of our findings with respect to the relationship between future changes in atmospheric circulation and air-quality related issues. These studies should make use of both high vertically resolved coupled atmosphere–ocean general circulation models and regional air-quality models. The former models are needed to better quantify anthropogenically induced changes in atmospheric circulation and their impacts on air quality, given the strong coupling between stratospheric and tropospheric circulation (e.g. Hoerling et al., 2001; Scaife et al., 2005; Omrani et al., 2013). The latter models can better constrain the effects of the altered atmospheric circulation on air quality at regional scales. The aerosol 2030 simulations used in this study assumed the MFR scenario; the extent to which these maximum-feasible air pollutant emission reductions will actually happen depends on the effectiveness of policies. Nevertheless, 60–70 % of the reduction (compared to a 2000

baseline) assumed by the MFR scenario is not unrealistic and hence some of the feedbacks seen in this study are likely to be witnessed in the real world. Most of the EU estimates of benefits related to pollution reduction (e.g. a decrease in the number of premature deaths) are determined without taking into account the potential effect of future atmospheric circulation changes. Therefore, more quantitative studies in which high-resolution regional air-quality models are coupled to global ocean–atmosphere–chemistry climate models are necessary to assess the climate feedbacks on aerosol abatement. Understanding and characterizing changes in the NAO in global models, thus, providing meteorological and chemical boundary conditions for regional air-quality models, will also allow for a better analysis of exceedance rates of air-quality standards associated with the inter-annual variability of circulation patterns.

Appendix A

In Appendix A, we explain in detail the relationship between the coherence index (CI) analysis and the NAO. The CI analysis of the SLP field identifies the areas that best correlate with the SLP variability over a given basin. In other words, the maxima in the CI represent the points that best capture SLP variability within a given domain. On the other hand, the NAOI is a measure of the wintertime SLP swings between two specific points in the North Atlantic, located in the "eye" of the two stable pressure areas, the Azores high and Icelandic low. Therefore, these two locations capture a substantial amount of SLP variability in the basin. Pausata et al. (2009) have already shown that the CI and the NAOI are connected to each other in the present climate. The CI patterns of surface temperature (precipitation) closely resemble the correlation patterns between surface temperature (precipitation) and the leading Principal Component (PC1) of the SLP field (which is an alternative definition of the NAOI; see Figs. 7 and 8 in Pausata et al., 2009). To further demonstrate the link between the CI and NAOI, we have calculated the correlation between SLP and the leading PC of the SLP field, following Pausata et al. (2009). For simplicity, in this paper we have used the canonical definition of the NAOI, since the PC1 and NAOI in winter are highly correlated ($r > 0.90$, see also Hurrell, 1995). Figure A1 shows that the correlation between the PC1 and SLP is very similar to the CI pattern and the correlation maxima of both analyses are quite close to each other (cf. Figs. A1 and 1a). The advantage of the CI analysis compared to the PC/SLP (or temperature or precipitation) correlation analysis is that the CI analysis does not depend only on the leading mode of variability but directly integrates all other modes that directly affect the fluctuations of the analysed variable.

Pausata et al. (2009) have also shown that, during different climate states in which the leading mode of SLP variability (PC1) is less dominant (lower explained variability of the EOF1), the CI and the PC correlation patterns can be completely different. Therefore, we have decided to adopt the CI in addition to the canonical NAOI as a further metric to better understand and interpret large-scale circulation changes.

Appendix B

In Appendix B, we examine how the large-scale atmospheric indicators used in this study are related to the number of rainy days in DJF over Europe. PM concentrations at the surface can be affected by different factors such as precipitation or the thermal structure of the boundary layer. However, these factors are implicitly included in the large-scale changes in atmospheric circulation, i.e. the changes in the CI pattern, NAO phase and blocking events.

We focus on the average number of rainy days per month during winter, because the monthly aerosol concentrations
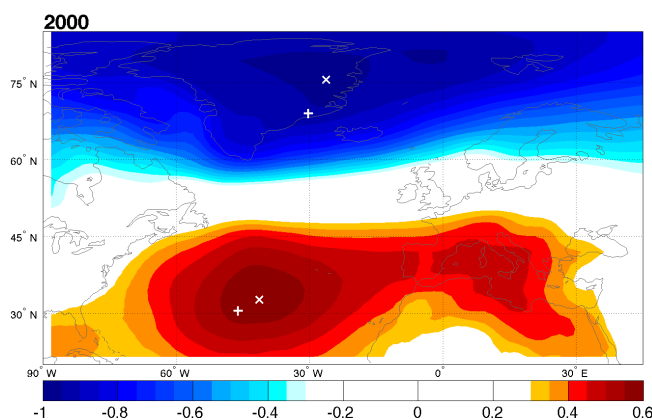
Figure A1. Correlations between North Atlantic winter SLP (December–February) and the PC1 of SLP. The markers indicate the maxima in CI (+ sign) and in the SLP/PC1 (x sign) correlations.

are more strongly affected by the number of rainy days (even with small precipitation amounts) rather than by the total intensity of the monthly precipitation (Claassen and Halm, 1995). We define a rainy day as a day with precipitation > 1 mm at a given gridbox.

In order to study the degree to which rainy day anomalies are associated to the NAO phase and the position of the southern SLP centre of action (SCOA) in the 2000 simulation, we use a regression analysis: a regression coefficient $b(i, j)$ is calculated at each specific latitude (i) and longitude (j) by linearly regressing the input variable of interest (e.g. rainy days (t, i, j), blocking frequency anomalies) against the reference time series (e.g. NAOI(t) or SCOA Index – SCOAI(t)).

The corresponding regression map is a composite field consisting of a linear combination of all available data, where each datum (e.g. rainy day/blocking frequency anomaly) is weighted by the concurrent value of the index (e.g. NAOI/SCOAI) time series:

$$b(i, j) = \left(\frac{1}{N}\right) \times \sum_{t=1}^{N} [\text{Rday}^{\text{anom}}(t, i, j) \times \text{INDEX}(t)], \quad \text{(B1)}$$

where N is the number of time samples. The $b(i, j)$ coefficients may be viewed as the perturbations in rainy day frequency at the (i, j)th grid point observed in association with a positive perturbation in the INDEX(t) (NAOI(t) or SCOAI(t)) by one standard deviation (i.e. NAOI/SCOAI = 1) (Lim and Wallace, 1991). For simplicity, we only show the anomalies associated with positive NAO (SCOA) phases; by construction, the anomaly pattern associated with the negative NAO phase differs only in sign. The regressions of the NAOI and SCOAI clearly show the influence of both the NAO phase and the position of the SCOA on rainy day frequency (Fig. B1). Positive NAO phases and SCOAs shifted to the east lead to decreased numbers of rainy days over
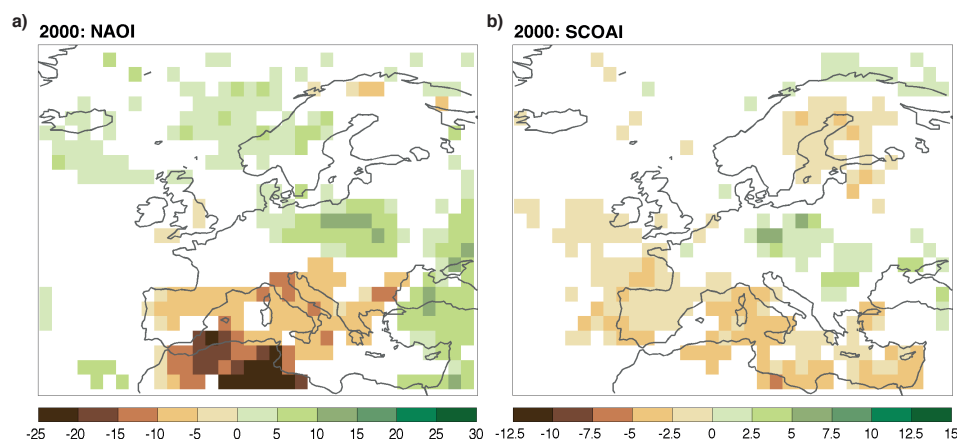
Figure B1. Rainy day anomalies (in %) per unit of NAOI **(a)** and CI time series **(b)** standard deviation. The CI time series has been constructed as described in Appendix B. The anomalies are calculated using a one-point regression analysis. Only differences significant at the 95 % confidence level are shown. Note that the two panels use different colour scales.
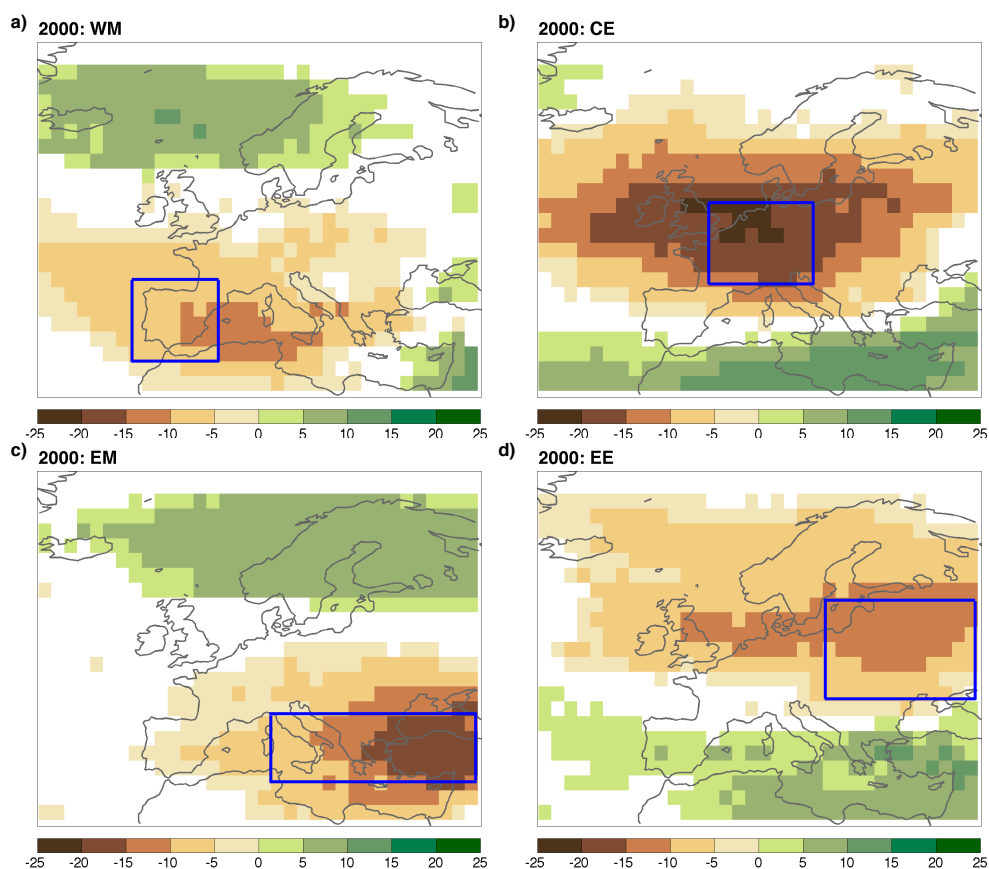
Figure B2. The values at each grid point show the composite anomaly in rainy days (in %) in the selected domain – WM **(a)**, CE **(b)**, EM **(c)**, EE **(d)** – while said grid point is blocked compared to the case where said grid point is unblocked. The composite is taken by averaging the rainy day anomaly maps obtained for each gridbox within the selected domain. For example, in panel **(a)** (WM) the positive values over southern Norway indicate that, when there is a blocking event there, rainy days over the WM increase by about 10 % compared to the case with no blocking over southern Norway. On the other hand, blocking events west and over the WM lead to 10–15 % precipitation anomalies relative to the case with no blocking events over the same regions. The regional domains analysed in each panel are marked by the blue rectangles.

the central-western Mediterranean and increases over part of central Europe. The opposite influence is found for the eastern Mediterranean, where a positive NAO phase is associated with an increased number of rainy days, while an eastward location of the southern SLP maximum is linked to a decreased number of rainy days.

Finally, we relate rainy day anomalies in each of the four selected regions in Europe (WM, EM, CE and EE) to the frequency of blocking events in the Atlantic sector (30–72° N, 80° W–45° E). To do so, we construct a composite map for each domain. We take each grid point (X_{fd}, Y_{fd}) within the full domain (entire Atlantic sector), and compute the frequency of rainy days at each grid point (x_{rd}, y_{rd}) within the regional domain (WM, EM, CE or EE) while grid point (X_{fd}, Y_{fd}) is blocked. Such values are assigned to grid point (X_{fd}, Y_{fd}). This calculation is then repeated for days on which grid point (X_{fd}, Y_{fd}) is unblocked. An anomaly in frequency of rainy days between the blocked and unblocked cases is then found. This means that, for each grid point (X_{fd}, Y_{fd}) in the full domain, we have several percentage anomalies, one for each grid point (x_{rd}, y_{rd}) within the regional domain. To obtain the composite map for each regional domain, we then average these values so that a single percentage value is assigned to each grid point (X_{fd}, Y_{fd}). For example, for WM the positive values over southern Norway indicate that, when there is a blocking event over this area, an increase in rainy days by about 10 % is expected over the WM compared to the case with no blocking over southern Norway. The value of 10 % is an average over the response at each of the grid points (x_{rd}, y_{rd}) within the WM domain. On the other hand, blocking events to the west of and over the WM lead to a 10–15 % increase in rainy days relative to the case with no blocking events over the same regions (Fig. B2a).

Hence, our analysis shows, as expected, that increased numbers of blocking events over western Europe and the eastern North Atlantic are associated with reduced numbers of rainy days over the Iberian Peninsula, while high-latitude blockings are associated with more precipitation days over the WM (Fig. B2a). For the EM, on the opposite, the blocking frequency over western Europe and the eastern North Atlantic does not have a remarkable influence (Fig. B2c). This, together with a contrasting influence on this region of the NAO and SCOA shifts (Fig. B1), may be responsible for the sometimes apparently ambiguous change in PM anomalies simulated in the three 2030 experiments.

This analysis shows how rainy days are connected to the large-scale circulation patterns investigated in this study, providing a context for their impact on PM concentrations at the surface.

Appendix C

In Appendix C, we examine how the number of rainy days in DJF changes in the 2030 simulations compared to the 2000 control experiment over Europe. This step will provide a better understanding of how the atmospheric circulation changes may impact – through changes in the number of rainy days – PM distributions in the future.

The 2030 simulation shows a clear dipole pattern, with an increased number of rainy days (up to 60 %) in central-northern Europe and a reduction (up to 50 %) in southern Europe, relative to 2000 simulation (Fig. C1). In general, similar patterns are found in the 2030GHG and 2030AER cases. However, there are some remarkable differences over the British Isles, central Europe and southern Norway, as well as the Mediterranean Basin. The increase in rainy days in the 2030AER seems to be shifted further south compared to the 2030GHG, leading to more rainy days over the British Isles and central Europe (2030AER) instead of the northern North Atlantic and southern Norway (2030GHG). The 2030AER simulation further shows a significant decrease in rainy days confined to the central-western part of the Mediterranean and to the southern North Atlantic, whereas in the 2030GHG the decrease is spread out over the entire Mediterranean. The combination of the 2030GHG and 2030AER changes in rainy days resembles the 2030 anomaly pattern (Fig. C1). The difference between the 2030GHG and 2030AER anomalies is likely related to the different changes in atmospheric circulations discussed in Sects. 3.1 and 3.2. The 2030GHG case experiences a more pronounced shift in the NAO phase compared to the 2030AER simulation and no changes in the SCOA. The 2030AER, on the other hand, is characterized by a significant eastward shift of the SCOA but only a small shift in the NAO (see Appendix B).
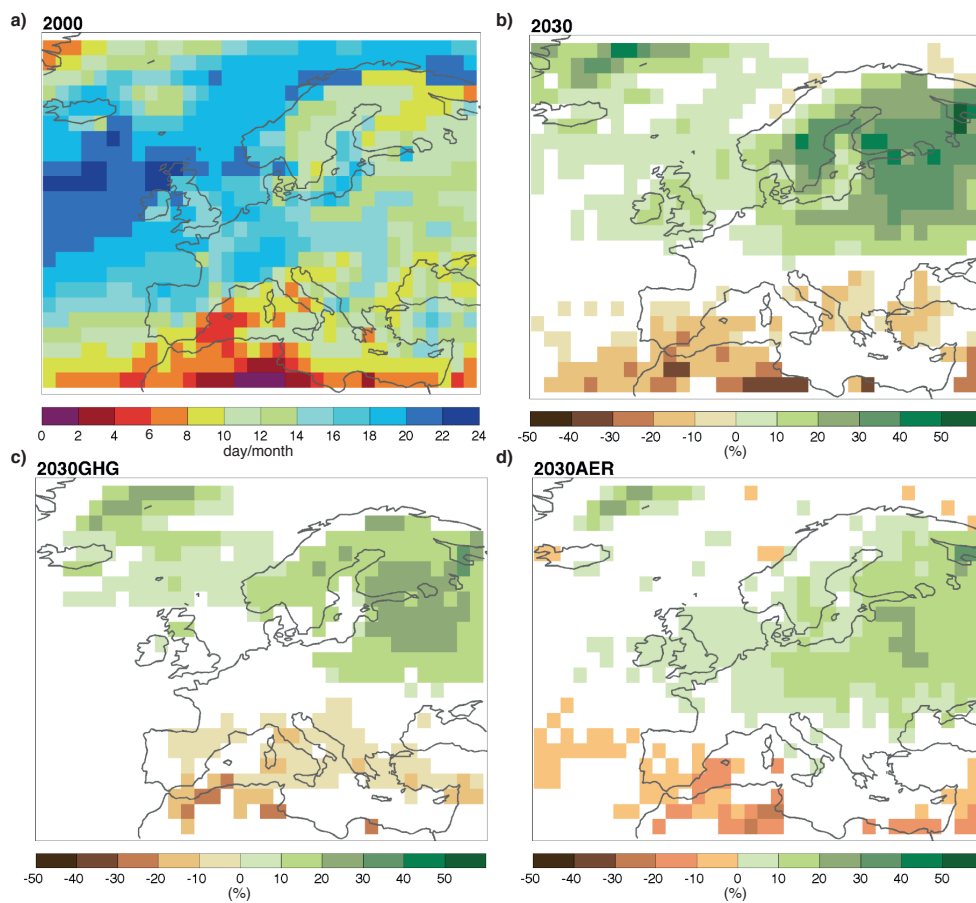
Figure C1. Average number of rainy days per month during winter (DJF) in the 2000 simulation (**a**). Percentage changes in the average number of rainy days per month for 2030 (**b**), 2030GHG (**c**), and 2030AER (**d**) simulations during winter. Only differences significant at the 95 % confidence level are shown.

References

Albrecht, B. A.: Aerosols, cloud microphysics, and fractional cloudiness, Science, 245, 1227–30, doi:10.1126/science.245.4923.1227, 1989.

Barnes, E. A. and Fiore, A. M.: Surface ozone variability and the jet position: Implications for projecting future air quality, Geophys. Res. Lett., 40, 2839–2844, doi:10.1002/grl.50411, 2013.

Barth, M. C., Rasch, P. J., Kiehl, J. T., Benkovitz, C. M., and Schwartz, S. E.: Sulfur chemistry in the National Center for Atmospheric Research Community Climate Model: Description, evaluation, features, and sensitivity to aqueous chemistry, J. Geophys. Res., 105, 1387, doi:10.1029/1999JD900773, 2000.

Berrisford, P., Hoskins, B. J., and Tyrlis, E.: Blocking and Rossby Wave Breaking on the Dynamical Tropopause in the Southern Hemisphere, J. Atmos. Sci., 64, 2881–2898, doi:10.1175/JAS3984.1, 2007.

Cagnazzo, C., Manzini, E., Giorgetta, M. A., Forster, P. M. De F., and Morcrette, J. J.: Impact of an improved shortwave radiation scheme in the MAECHAM5 General Circulation Model, Atmos. Chem. Phys., 7, 2503–2515, doi:10.5194/acp-7-2503-2007, 2007.

Christoudias, T., Pozzer, A., and Lelieveld, J.: Influence of the North Atlantic Oscillation on air pollution transport, Atmos. Chem. Phys., 12, 869–877, doi:10.5194/acp-12-869-2012, 2012.

Claassen, H. C. and Halm, D. R.: A possible deficiency in estimates of wet deposition obtained from data generated by the NADP/NTN network, Atmos. Environ., 29, 437–448, doi:10.1016/1352-2310(94)00182-K, 1995.

Cofala, J., Amann, M., Klimont, Z., Kupiainen, K., and Höglund-Isaksson, L.: Scenarios of global anthropogenic emissions of air pollutants and methane until 2030, Atmos. Environ., 41, 8486–8499, doi:10.1016/j.atmosenv.2007.07.010, 2007.

Croci-Maspoli, M., Schwierz, C., and Davies, H. C.: Atmospheric blocking: space-time links to the NAO and PNA, Clim. Dyn., 29, 713–725, doi:10.1007/s00382-007-0259-4, 2007.

Davini, P. and Cagnazzo, C.: On the misinterpretation of the North Atlantic Oscillation in CMIP5 models, Clim. Dyn., 43, 1497–1511, doi:10.1007/s00382-013-1970-y, 2013.

Davini, P., Cagnazzo, C., Gualdi, S., and Navarra, A.: Bidimensional Diagnostics, Variability, and Trends of Northern Hemisphere Blocking, J. Clim., 25, 6496–6509, doi:10.1175/JCLI-D-12-00032.1, 2012.

Eckhardt, S., Stohl, A., Beirle, S., Spichtinger, N., James, P., Forster, C., Junker, C., Wagner, T., Platt, U., and Jennings, S. G.: The North Atlantic Oscillation controls air pollution transport to the Arctic, Atmos. Chem. Phys., 3, 1769–1778, doi:10.5194/acp-3-1769-2003, 2003.

EEA: European Environment Agency: Air quality in Europe, Tech. rep., Luxembourg, Publications Office of the European Union., available at: http://www.eea.europa.eu/publications/air-quality-in-europe-2013, 2013.

Feichter, J., Kjellström, E., Rodhe, H., Dentener, F., Lelieveld, J., and Roelofs, G.-J.: Simulation of the tropospheric sulfur cycle in a global climate model, Atmos. Environ., 30, 1693–1707, doi:10.1016/1352-2310(95)00394-0, 1996.

Feichter, J., Roeckner, E., Lohmann, U., and Liepert, B.: Nonlinear Aspects of the Climate Response to Greenhouse Gas and Aerosol Forcing, J. Clim., 17, 2384–2398, doi:10.1175/1520-0442(2004)017<2384:NAOTCR>2.0.CO;2, 2004.

Fiore, A. M., Naik, V., Spracklen, D. V, Steiner, A., Unger, N., Prather, M., Bergmann, D., Cameron-Smith, P. J., Cionni, I., Collins, W. J., Dalsøren, S., Eyring, V., Folberth, G. A., Ginoux, P., Horowitz, L. W., Josse, B., Lamarque, J.-F., MacKenzie, I. A., Nagashima, T., O'Connor, F. M., Righi, M., Rumbold, S. T., Shindell, D. T., Skeie, R. B., Sudo, K., Szopa, S., Takemura, T., and Zeng, G.: Global air quality and climate., Chem. Soc. Rev., 41, 6663–83, doi:10.1039/c2cs35095e, 2012.

Fischer-Bruns, I., Banse, D. F., and Feichter, J.: Future impact of anthropogenic sulfate aerosol on North Atlantic climate, Clim. Dyn., 32, 511–524, doi:10.1007/s00382-008-0458-7, 2008.

Gillett, N. P. and Fyfe, J. C.: Annular mode changes in the CMIP5 simulations, Geophys. Res. Lett., 40, 1189–1193, doi:10.1002/grl.50249, 2013.

Gleckler, P. J., Taylor, K. E., and Doutriaux, C.: Performance metrics for climate models, J. Geophys. Res., 113, D06104, doi:10.1029/2007JD008972, 2008.

Hilmer, M. and Jung, T.: Evidence for a recent change in the link between the North Atlantic Oscillation and Arctic Sea ice export, Geophys. Res. Lett., 27, 989–992, doi:10.1029/1999GL010944, 2000.

Hoerling, M. P., Hurrell, J. W., and Xu, T.: Tropical origins for recent North Atlantic climate change, Science, 292, 90–92, doi:10.1126/science.1058582, 2001.

Hori, M. E., Nohara, D., and Tanaka, H. L.: Influence of Arctic Oscillation towards the Northern Hemisphere Surface Temperature Variability under the Global Warming Scenario, J. Meteorol. Soc. Japan, 85, 847–859, doi:10.2151/jmsj.85.847, 2007.

Horton, D. E., Skinner, C. B., Singh, D., and Diffenbaugh, N. S.: Occurrence and persistence of future atmospheric stagnation events, Nat. Clim. Chang., 4, 698–703, doi:10.1038/nclimate2272, 2014.

Hu, Z.-Z. and Wu, Z.: The intensification and shift of the annual North Atlantic Oscillation in a global warming scenario simulation, Tellus A, 56, 112–124, doi:10.1111/j.1600-0870.2004.00050.x, 2004.

Hurrell, J. W.: Decadal trends in the north atlantic oscillation: regional temperatures and precipitation, Science, 269, 676–679, doi:10.1126/science.269.5224.676, 1995.

IMAGE-team: The IMAGE 2.2 implementation of the SRES scenarios. A comprehensive analysis of emissions, climate change and impacts in the 21st century, CD-ROM Publ., Bilthoven, Natl. Inst. Public Heal. Environ., 2001.

IPCC: Climate Change 2013: The Physical Science Basis. Contribution of Working Group I to the Fifth Assessment Report of the Intergovernmental Panel on Climate Change, edited by: T. F. Stocker, D. Qin, G.-K. Plattner, M. Tignor, S. K. Allen, J. Boschung, A. Nauels, Y. Xia, V. Bex, and P. M. Midgley, Cam-

bridge University Press, Cambridge, United Kingdom and New York, NY, USA, 2013.

Jacob, D. J. and Winner, D. A.: Effect of Climate Change on Air Quality, Atmos. Environ., 43, 51–63, available at: http://dash.harvard.edu/handle/1/3553961 (last access: 9 October 2014), 2009.

Karpechko, A. Y.: Uncertainties in future climate attributable to uncertainties in future Northern Annular Mode trend, Geophys. Res. Lett., 37, L20702, doi:10.1029/2010GL044717, 2010.

Kloster, S., Dentener, F., Feichter, J., Raes, F., van Aardenne, J., Roeckner, E., Lohmann, U., Stier, P., and Swart, R.: Influence of future air pollution mitigation strategies on total aerosol radiative forcing, Atmos. Chem. Phys., 8, 6405–6437, doi:10.5194/acp-8-6405-2008, 2008.

Kloster, S., Dentener, F., Feichter, J., Raes, F., Lohmann, U., Roeckner, E., and Fischer-Bruns, I.: A GCM study of future climate response to aerosol pollution reductions, Clim. Dyn., 34, 1177–1194, doi:10.1007/s00382-009-0573-0, 2009.

Kuzmina, S. I.: The North Atlantic Oscillation and greenhouse-gas forcing, Geophys. Res. Lett., 32, L04703, doi:10.1029/2004GL021064, 2005.

Lim, G. H. and Wallace, J. M.: Structure and Evolution of Baroclinic Waves as Inferred from Regression Analysis, J. Atmos. Sci., 48, 1718–1732, doi:10.1175/1520-0469(1991)048<1718:SAEOBW>2.0.CO;2, 1991.

Lim, S. S., Vos, T., Flaxman, A. D., Danaei, G., Shibuya, K., Adair-Rohani, H., Amann, M., Anderson, H. R., Andrews, K. G., Aryee, M., Atkinson, C., Bacchus, L. J., Bahalim, A. N., Balakrishnan, K., Balmes, J., Barker-Collo, S., Baxter, A., Bell, M. L., Blore, J. D., Blyth, F., Bonner, C., Borges, G., Bourne, R., Boussinesq, M., Brauer, M., Brooks, P., Bruce, N. G., Brunekreef, B., Bryan-Hancock, C., Bucello, C., Buchbinder, R., Bull, F., Burnett, R. T., Byers, T. E., Calabria, B., Carapetis, J., Carnahan, E., Chafe, Z., Charlson, F., Chen, H., Chen, J. S., Cheng, A. T.-A., Child, J. C., Cohen, A., Colson, K. E., Cowie, B. C., Darby, S., Darling, S., Davis, A., Degenhardt, L., Dentener, F., Des Jarlais, D. C., Devries, K., Dherani, M., Ding, E. L., Dorsey, E. R., Driscoll, T., Edmond, K., Ali, S. E., Engell, R. E., Erwin, P. J., Fahimi, S., Falder, G., Farzadfar, F., Ferrari, A., Finucane, M. M., Flaxman, S., Fowkes, F. G. R., Freedman, G., Freeman, M. K., Gakidou, E., Ghosh, S., Giovannucci, E., Gmel, G., Graham, K., Grainger, R., Grant, B., Gunnell, D., Gutierrez, H. R., Hall, W., Hoek, H. W., Hogan, A., Hosgood, H. D., Hoy, D., Hu, H., Hubbell, B. J., Hutchings, S. J., Ibeanusi, S. E., Jacklyn, G. L., Jasrasaria, R., Jonas, J. B., Kan, H., Kanis, J. A., Kassebaum, N., Kawakami, N., Khang, Y.-H., Khatibzadeh, S., Khoo, J.-P., Kok, C., et al.: A comparative risk assessment of burden of disease and injury attributable to 67 risk factors and risk factor clusters in 21 regions, 1990–2010: a systematic analysis for the Global Burden of Disease Study 2010, Lancet, 380, 2224–2260, doi:10.1016/S0140-6736(12)61766-8, 2012.

Lohmann, U., Stier, P., Hoose, C., Ferrachat, S., Kloster, S., Roeckner, E., and Zhang, J.: Cloud microphysics and aerosol indirect effects in the global climate model ECHAM5-HAM, Atmos. Chem. Phys., 7, 3425–3446, doi:10.5194/acp-7-3425-2007, 2007.

Müller, W. A. and Roeckner, E.: ENSO teleconnections in projections of future climate in ECHAM5/MPI-OM, Clim. Dyn., 31, 533–549, doi:10.1007/s00382-007-0357-3, 2008.

Nakicenovic N. and Swart R.: Special Report on Emissions Scenarios: A Special Report of Working Group III of the Intergovernmental Panel on Climate Change, Cambridge University Press, Cambridge, UK, ISBN:9780521804936, 2000.

Nazarenko, L. and Menon, S.: Varying trends in surface energy fluxes and associated climate between 1960 and 2002 based on transient climate simulations, Geophys. Res. Lett., 32, L22704, doi:10.1029/2005GL024089, 2005.

Omrani, N.-E., Keenlyside, N. S., Bader, J., and Manzini, E.: Stratosphere key for wintertime atmospheric response to warm Atlantic decadal conditions, Clim. Dyn., 42, 649–663, doi:10.1007/s00382-013-1860-3, 2013.

Pausata, F. S. R., Li, C., Wettstein, J. J., Nisancioglu, K. H., and Battisti, D. S.: Changes in atmospheric variability in a glacial climate and the impacts on proxy data: a model intercomparison, Clim. Past, 5, 489–502, doi:10.5194/cp-5-489-2009, 2009.

Pausata, F. S. R., Pozzoli, L., Vignati, E., and Dentener, F. J.: North Atlantic Oscillation and tropospheric ozone variability in Europe: model analysis and measurements intercomparison, Atmos. Chem. Phys., 12, 6357–6376, doi:10.5194/acp-12-6357-2012, 2012.

Pausata, F. S. R., Pozzoli, L., Dingenen, R. Van, Vignati, E., Cavalli, F., and Dentener, F. J.: Impacts of changes in North Atlantic atmospheric circulation on particulate matter and human health in Europe, Geophys. Res. Lett., 40, 4074–4080, doi:10.1002/grl.50720, 2013.

Pelly, J. L. and Hoskins, B. J.: A New Perspective on Blocking, J. Atmos. Sci., 60, 743–755, doi:10.1175/1520-0469(2003)060<0743:ANPOB>2.0.CO;2, 2003.

Peterson, K. A., Lu, J., and Greatbatch, R. J.: Evidence of nonlinear dynamics in the eastward shift of the NAO, Geophys. Res. Lett., 30, 1030, doi:10.1029/2002GL015585, 2003.

Pham, M.: Changes in atmospheric sulfur burdens and concentrations and resulting radiative forcings under IPCC SRES emission scenarios for 1990–2100, J. Geophys. Res., 110, D06112, doi:10.1029/2004JD005125, 2005.

Rex, D. F.: Blocking Action in the Middle Troposphere and its Effect upon Regional Climate, Tellus, 2, 196–211, doi:10.1111/j.2153-3490.1950.tb00331.x, 1950.

Riahi, K. and Roehrl, R. A.: Greenhouse Gas Emissions in a Dynamics-as-Usual Scenario of Economic and Energy Development, Technol. Forecast. Soc. Change, 63, 175–205, doi:10.1016/S0040-1625(99)00111-0, 2000.

Roeckner, E., Siebert, T., and Feichter, J.: Climatic response to anthropogenic sulfate forcing simulated with a general circulation model, in Aerosol Forcing of Climate, edited by R. J. Charlson and J. Heintzenberg, 349–362, John Wiley & Sons Ltd., Chichester., 1995.

Roeckner, E., Bengtsson, L., Feichter, J., Lelieveld, J., and Rodhe, H.: Transient Climate Change Simulations with a Coupled Atmosphere–Ocean GCM Including the Tropospheric Sulfur Cycle, J. Clim., 12, 3004–3032, doi:10.1175/1520-0442(1999)012<3004:TCCSWA>2.0.CO;2, 1999.

Roeckner, E., Bäuml, G., Bonaventura, L., Brokopf, R., Esch, M., Giorgetta, M., Hagemann, S., Kirchner, I., Kornblueh, L., Manzini, E., Rhodin, A., Schlese, U., Schulzweida, U. and Tompkins, A.: The atmospheric general circulation model ECHAM5 – Part I: Model description, Tech. Rep. 349, Max-Planck-Institut für Meteorologie, Hamburg, Germany, 2003.

Roelofs, G.-J., Lelieveld, J., and Ganzeveld, L.: Simulation of global sulfate distribution and the influence on effective cloud drop radii with a coupled photochemistry sulfur cycle model, Tellus B, 50, doi:10.3402/tellusb.v50i3.16098, 1998.

Rosenblatt, M.: Remarks on Some Nonparametric Estimates of a Density Function, Ann. Math. Stat., 27, 832–837, 1956.

Scaife, A. A., Knight, J. R., Vallis, G. K., and Folland, C. K.: A stratospheric influence on the winter NAO and North Atlantic surface climate, Geophys. Res. Lett., 32, L18715, doi:10.1029/2005GL023226, 2005.

Shindell, D., Kuylenstierna, J. C. I., Vignati, E., van Dingenen, R., Amann, M., Klimont, Z., Anenberg, S. C., Muller, N., Janssens-Maenhout, G., Raes, F., Schwartz, J., Faluvegi, G., Pozzoli, L., Kupiainen, K., Höglund-Isaksson, L., Emberson, L., Streets, D., Ramanathan, V., Hicks, K., Oanh, N. T. K., Milly, G., Williams, M., Demkine, V., and Fowler, D.: Simultaneously mitigating near-term climate change and improving human health and food security, Science, 335, 183–189, doi:10.1126/science.1210026, 2012.

Sillmann, J., Pozzoli, L., Vignati, E., Kloster, S. and Feichter, J.: Aerosol effect on climate extremes in Europe under different future scenarios, Geophys. Res. Lett., 40, 2290–2295, doi:10.1002/grl.50459, 2013.

Stephenson, D. B., Pavan, V., Collins, M., Junge, M. M., and Quadrelli, R.: North Atlantic Oscillation response to transient greenhouse gas forcing and the impact on European winter climate: a CMIP2 multi-model assessment, Clim. Dyn., 27, 401–420, doi:10.1007/s00382-006-0140-x, 2006.

Stier, P., Feichter, J., Kinne, S., Kloster, S., Vignati, E., Wilson, J., Ganzeveld, L., Tegen, I., Werner, M., Balkanski, Y., Schulz, M., Boucher, O., Minikin, A., and Petzold, A.: The aerosol–climate model ECHAM5-HAM, Atmos. Chem. Phys., 5, 1125–1156, doi:10.5194/acp-5-1125-2005, 2005.

Sundquist, H., Berge, E.. and Kristjansson, J. E.: Condensation and cloud parameterization studies with a mesoscale numerical prediction model, Mon. Weather Rev., 117, 1641–1657, 1989.

Textor, C., Schulz, M., Guibert, S., Kinne, S., Balkanski, Y., Bauer, S., Berntsen, T., Berglen, T., Boucher, O., Chin, M., Dentener, F., Diehl, T., Feichter, J., Fillmore, D., Ginoux, P., Gong, S., Grini, A., Hendricks, J., Horowitz, L., Huang, P., Isaksen, I. S. A., Iversen, T., Kloster, S., Koch, D., Kirkevåg, A., Kristjansson, J. E., Krol, M., Lauer, A., Lamarque, J. F., Liu, X., Montanaro, V., Myhre, G., Penner, J. E., Pitari, G., Reddy, M. S., Seland, Ø., Stier, P., Takemura, T., and Tie, X.: The effect of harmonized emissions on aerosol properties in global models – an AeroCom experiment, Atmos. Chem. Phys., 7, 4489–4501, doi:10.5194/acp-7-4489-2007, 2007.

Tibaldi, S. and Molteni, F.: On the operational predictability of blocking, Tellus A, 42, 343–365, doi:10.1034/j.1600-0870.1990.t01-2-00003.x, 1990.

Toon, O. B. and Ackerman, T. P.: Algorithms for the calculation of scattering by stratified spheres., Appl. Opt., 20, 3657–3660, doi:10.1364/AO.20.003657, 1981.

Twomey, S.: The Influence of Pollution on the Shortwave Albedo of Clouds, J. Atmos. Sci., 34, 1149–1152, 1977.

Vignati, E., Wilson, J., and Stier, P.: M7: An efficient size-resolved aerosol microphysics module for large-scale aerosol transport models, J. Geophys. Res., 109, D22202, doi:10.1029/2003JD004485, 2004.

Walker, G. T. and Bliss, E. W.: World weather V, Mem. R. Meteorol. Soc., 4, 53–84, 1932.

Wang, Y.-H. and Magnusdottir, G.: The Shift of the Northern Node of the NAO and Cyclonic Rossby Wave Breaking, J. Clim., 25, 7973–7982, doi:10.1175/JCLI-D-11-00596.1, 2012.

WHO: Review of evidence on health aspects of air pollution – REVIHAAP Project. First results., Tech. rep., Copenhagen, World Health Organization, 2013.

Woollings, T., Hoskins, B., Blackburn, M. and Berrisford, P.: A New Rossby Wave – Breaking Interpretation of the North Atlantic Oscillation, J. Atmos. Sci., 65, 609–626, doi:10.1175/2007JAS2347.1, 2008.

Yao, Y. and Luo, D.: Relationship between zonal position of the North Atlantic Oscillation and Euro-Atlantic blocking events and its possible effect on the weather over Europe, Sci. China Earth Sci., doi:10.1007/s11430-014-4949-6, 2014.

Yiou, P. and Nogaj, M.: Extreme climatic events and weather regimes over the North Atlantic: When and where?, Geophys. Res. Lett., 31, L07202, doi:10.1029/2003GL019119, 2004.